Biofabrication

PAPER

Drug compound screening in single and integrated multi-organoid body-on-a-chip systems

RECEIVED
18 October 2019

REVISED
13 December 2019

ACCEPTED FOR PUBLICATION
17 January 2020

PUBLISHED
26 February 2020

Aleksander Skardal[1,2,4], **Julio Aleman**[1], **Steven Forsythe**[1], **Shiny Rajan**[1], **Sean Murphy**[1], **Mahesh Devarasetty**[1], **Nima Pourhabibi Zarandi**[1], **Goodwell Nzou**[1], **Robert Wicks**[1], **Hooman Sadri-Ardekani**[1], **Colin Bishop**[1], **Shay Soker**[1], **Adam Hall**[3], **Thomas Shupe**[1] and **Anthony Atala**[1,4]

[1] Wake Forest Institute for Regenerative Medicine, Wake Forest School of Medicine, Medical Center Boulevard, Winston-Salem, NC, 27101, United States of America
[2] Department of Biomedical Engineering, The Ohio State University, 1080 Carmack Road, Columbus, OH, 43210, United States of America
[3] Department of Biomedical Engineering, Wake Forest School of Medicine, Medical Center Boulevard, Winston-Salem, NC, 27157, United States of America
[4] Authors to whom any correspondence should be addressed.

E-mail: skardal.1@osu.edu **and** aatala@wakehealth.edu

Keywords: organoids, tissue chips, body-on-a-chip, *in vitro* drug screening

Supplementary material for this article is available online

Abstract

Current practices in drug development have led to therapeutic compounds being approved for widespread use in humans, only to be later withdrawn due to unanticipated toxicity. These occurrences are largely the result of erroneous data generated by *in vivo* and *in vitro* preclinical models that do not accurately recapitulate human physiology. Herein, a human primary cell- and stem cell-derived 3D organoid technology is employed to screen a panel of drugs that were recalled from market by the FDA. The platform is comprised of multiple tissue organoid types that remain viable for at least 28 days, *in vitro.* For many of these compounds, the 3D organoid system was able to demonstrate toxicity. Furthermore, organoids exposed to non-toxic compounds remained viable at clinically relevant doses. Additional experiments were performed on integrated multi-organoid systems containing liver, cardiac, lung, vascular, testis, colon, and brain. These integrated systems proved to maintain viability and expressed functional biomarkers, long-term. Examples are provided that demonstrate how multi-organoid 'body-on-a-chip' systems may be used to model the interdependent metabolism and downstream effects of drugs across multiple tissues in a single platform. Such 3D *in vitro* systems represent a more physiologically relevant model for drug screening and will likely reduce the cost and failure rate associated with the approval of new drugs.

1. Introduction

The development of new drugs can take a decade and a half, from preclinical studies to reaching the market. It is estimated that only one in 5000 drug candidates is able to successfully complete this journey [1]. Additionally, the cost for bringing a single drug to market, with all direct and indirect expenses accounted for, can climb as high as $2.6 billion . Unfortunately, the human and financial costs can be even more dramatic if a drug is later found to be harmful and must be withdrawn [2] . For example, Vioxx (Rofecoxib), a COX-2 selective inhibitor NSAID developed by Merck & Co. was forced to pay $4.85 billion to settle 27 000 cases and another $830 million dollars to settle shareholder lawsuits. These settlements stemmed from a large number of adverse events that were determined to have occurred as a result of Merck's failure to properly evaluate the drug [2, 3]. In addition to the monetary costs, the human costs of adverse drug reactions are a leading cause of hospitalization in the United States, as up to 5.3% of hospitalizations are related to adverse drug reactions [4]. The rate of fatal adverse drug reactions is difficult to determine, and it is probable that these events are under-reported, with one study estimating that these reactions are the fourth

highest cause of death in the United States [5]. As both adverse human effects and drug development costs increase, access to more reliable and affordable drug screening tools becomes more critical.

Traditional *in vitro* 2D cultures have been the foundation of countless scientific discoveries, but may not always accurately recapitulate the *in vivo* 3D cellular microenvironment [6]. Cells grown in 2D experience foreign surface topography, substrate stiffness, cell-cell/cell-matrix interactions, and availability of soluble bioregulatory factors, as compared to 3D systems. As such, cell maintenance under 2D conditions can substantially alter the transcriptome and proteome, producing experimental outcomes that may not be representative of *in vivo* cellular physiology [7, 8]. For example, normal primary human liver cell types demonstrated vastly superior viability and function when incorporated into liver organoids, as compared to 2D cultures comprised of these exact same cells [9, 10]. Animal models used for preclinical drug studies have major limitations, as these can be expensive, are difficult to control, and often fail to accurately model human metabolism, drug efficacy and immune function [11]. Bioengineered 3D cellular platforms, such as tissue organoids comprised of human primary and stem cell-derived cells, mimic many of the microenvironmental conditions present in native human tissue, and thus may be a superior tool for preclinical research and translational medicine.

Significant research efforts have been directed towards developing suitable models for the two organs most frequently affected by adverse drug reactions: heart and liver. Cardiac toxicity is responsible for 31% of all adverse drug reactions, with a majority of these affecting either calcium or potassium channels, resulting in arrhythmias [12]. Several models have been created for testing cytotoxicity resulting from impaired channel function *in vitro*, but these 3D models are generally comprised of a single cell type [13–16]. The liver is the most important organ in terms of drug metabolism, due to robust expression of both phase I & II metabolism enzymes, such as cytochrome p450s and transferases that modify xenobiotic compounds to excretable forms [17, 18]. Often when drugs are recalled, it is due to unpredicted metabolism of the compound. For example, differences in rat and human physiology, such as an overlap of only several cytochrome p450 isoforms, and failure to consider altered metabolism in obese patients, allowed for a market approval of troglitazone, which later may have contributed to many patients requiring liver transplants due to unexpected hepatotoxicity [19–21].

Even modern studies employing human tissue organoids often overlook the complex, integrated nature of the human body. *In vivo*, organs and tissues do not exist in isolation. Rather, they exist in a dynamic interconnected system, in which, they interact and support one another. There are now several published studies where multiple tissue types are integrated within a multi-organoid, *in-vitro* platform [9, 22–28]. While these systems have pushed organ-on-a-chip technology significantly forward over the past several years, we are still a long way from a true 'body-on-a-chip' system. Moreover, these studies have largely been based upon animal-derived cells, immortalized cell lines, or 2D cultures of primary human cells, rather than high functioning 3D organoids with tissue constructs comprised of human primary or stem cell-derived cell populations that act as miniaturized surrogates of their *in vivo* counterparts.

To address these shortcomings, we tested 3D organoids previously designed and optimized in our laboratory [9] with a panel of recalled drugs that caused adverse effects to the liver and heart in human subjects. These compounds passed through 2D *in vitro* studies, animal studies, and clinical trials, and were made available to the general public. These drugs were intended to treat a wide range of ailments and were found to cause serious adverse effects once approved for use in humans. In the current study, these compounds were screened in 3D liver and cardiac organoid platforms, and results were compared to those generated in 2D cell culture systems, as well as cell lines in both 2D and 3D. In order to model the integrated nature of the human body, our previously described integrated 3-tissue platform [9] was expanded to support up to six individual tissue types under a common recirculating media. With this platform, we demonstrated that a complex system, containing a wide variety of individual human primary and stem cell-derived cell types, can be maintained as a viable and functional platform. Lastly, we describe integrated drug studies in which the presence of one organoid type is required for the manifestation of drug toxicity on downstream organoids.

2. Materials and methods

2.1. Liver and cardiac cell sources, culture, and organoid formation

All cells employed for liver and cardiac organoids were obtained from commercial sources, and were either human primary cells or human iPS cell-derived. Hepatic stellate cells (HSCs) (ScienCell, Carlsbad, CA) were first expanded for two passages in culture before organoid formation, or alternatively for cryopreservation for later rounds of organoid production. During these passages, HSCs were maintained using 90% DMEM (high glucose, ThermoFisher, Waltham, MA) and 10% fetal bovine serum (FBS, Atlanta Biologicals, Flowery Branch, GA) on a collagen I coating (10 μg cm^{-2}, Corning, Corning, NY) at 37 °C with 5% CO_2. Primary human hepatocytes (Triangle Research Labs, RTP, NC) were thawed according to manufacturer instructions using the proprietary Hepatocyte Thawing Medium (Triangle Research Labs). Kupffer cells were also thawed according to manufacturer

instructions (Gibco, Waltham, MA). Cells were then harvested using trypsin and either used in organoid formation or placed into a 96-well plate at 1500 cells per well and then immediately used in experiments. For single organoid drug studies, two-dimensional (2D) hepatocyte matrix sandwich cultures were used as a comparison to the 3D liver organoids. In these sandwich cultures, primary human hepatocytes were thawed as described, then plated on collagen coated (10 μg cm^{-2}, Corning) 6-well culture plates, using Hepatocyte Plating medium (Triangle Research Labs) at a density of ~150 000 cells cm^{-2}. Cells were placed in the incubator at 37 °C with 5% CO_2 for 4 h before Matrigel was added as a top layer (BD Biosciences, San Jose, CA). After an additional 24 h incubation, fresh HCM medium was added (Lonza, Walkersville, MD).

Induced pluripotent stem cell-derived cardiomyocytes (iPSC CMs) were purchased from Axiogenesis (cat. # COR.4U Cardiomyocytes). Human primary cardiac fibroblasts were purchased from ScienCell (cat. # 6330). Before initiating organoid preparation, iPSC CMs were seeded on tissue culture plastic and maintained for 48 h in COR.4U medium until the cells began to beat spontaneously in a synchronized fashion. iPSC CMs were then retrieved from culture using trypsin-EDTA (Hyclone, Logan, UT) and employed directly for organoid formation or plated into 96-well plate at 1000 cells per well and then immediately used for experimentation.

Liver and cardiac organoids were formed by aggregation using 96-well format non-adherent round bottom plates. For liver organoids cells were combined in a media mixture comprised of 90% HCM medium (Lonza), 10% heat-inactivated fetal bovine serum (Gibco), and rat tail collagen I (10 ng μl^{-1}, Corning). Liver organoids were produced by preparing a cell suspension mixture of 80% hepatocytes (Triangle Research Labs), 10% hepatic stellate cells (ScienCell), and 10% Kupffer cells (Gibco). Droplets of 40 μl media containing approximately 1500 cells were placed in each well of a non-adherent, round-bottom, 96-well plates and allowed to aggregate into organoids. Cardiac organoids were produced in a similar manner. IPSC CMs were suspended in cardiomyocyte maintenance medium (CMM, Stem Cell Theranostics, Redwood City, CA). Fibroblasts were added to the cell suspension, making up approximately 10% of the total cell number, after which the fluid volume was adjusted so cell density was about 10 000 cells ml^{-1}. Subsequently, 100 μl of the cardiomyocyte and fibroblast containing cell suspension was pipetted into each well of the non-adherent, round-bottom, 96-well plates to produce organoids (#7007, Corning) to result in approximately 1000 cells/organoid. Well plates were incubated and observed daily until organoids formed, after which they were immediately employed in experiments.

2.2. Cell line maintenance for comparative drug studies

HepG2 and C2C12 cells were plated onto 15 cm culture dishes and placed inside 37 °C incubator until reaching 80% and 50% confluence, respectively. Media changes were performed every two days using DMEM with 10% FBS. Cells were removed using Trypsin at 0.05% for 5-minute at 37°C. Cells were then added to the wells of a 96-well plate in the same quantity as the organoid total, 1500 for HepG2 and 1000 for C2C12 cells, and then immediately used for experiments. To form 3D spheroids as a comparison, HepG2 or C2C12 cells were formed into spheroids as described above for primary liver organoids and iPSC-derived cardiac organoids.

2.3. Preparation of drug stock solutions

All ten recalled drugs were purchased from Sigma Aldrich (St. Louis, MO). Drugs were dissolved in DMSO to reach 10 mM concentration. A range of doses from 1 nM to 100 μM was utilized to determine IC_{50} values for each of the recalled drugs. Serial dilutions were performed in media for each cell type until all concentrations were created at 2X final concentration. Compounds were added in 100 μl volumes to the 100 μl of media already in the wells, and organoids were allowed to incubate for 2 days at 37 °C with 5% CO_2 prior to subsequent analyses described below. For drugs pergolide, rofecoxib, valdecoxib, bromfenac, tienilic acid and troglitazone, an additional stock of 100 mM solution was made to create a dose of 1 mM as no IC_{50} was determined using the initial doses tested. Non-toxic compounds aspirin, ibuprofen, ascorbic acid, loratadine, and quercetin were also purchased from Sigma Aldrich and prepared in a similar manner, resulting in concentrations ranging from 1 μM to 1 mM that were administered in the same manner described above.

2.4. Live/Dead staining

Organoids were isolated from 96-well low adhesion round bottom plates, suspended in Hystem hydrogel (GS311) in a 20 μl construct according to manufacturer's instructions (ESI-BIO, Almeida, California), and placed into 12-well plates. Media was then removed, and organoids were assessed by LIVE/DEAD® Viability/Cytotoxicity Kit assays (Invitrogen, Carlsbad, CA). Specifically, 2.0 μM calcein AM and 4.0 μM ethidium homodimer in PBS was added to each well and was allowed to incubate for 1 h. Imaging was then performed by macro-confocal microscopy (Leica TCS LSI, Leica, Wetzlar, Germany) and composite images were created with ethidium bromide red fluorescence representing dead nuclei and calcein AM green fluorescence representing live cells.

2.5. ATP activity assays

Following drug compound incubations, media was removed from each well, leaving 100 μl of media along with the organoid. Next, 100 μl of Cell-Titer Glo Luminescent Cell Viability Assay solution, prepared according to manufacturer's instructions (G7571, Promega, Madison, WI), was added to each well and incubated for 10 min at room temperature while shielded from light. The entire supernatant volume of the wells containing organoids was then added to Costar Black Polystrene 96-well Assay Plate wells and the contents were read on a Vertias Microplate Luminometer using default settings. Values were then averaged amongst the different groups and graphed for analysis. All conditions were performed with $n \geqslant 6$.

2.6. Heart beat assay

Fully formed cardiac organoids in the wells of a 96-well non-adhesive round bottom plate were placed under a Leica DMIL LED microscope to allow for the recording of baseline beat rates in 20 s videos ($\mathbf{n = 3}$). The plate was then returned to the 37 °C, 5% CO_2 incubator for five minutes to ensure that organoids did not experience significant temperature decreases. The process was repeated until all experimental organoids exposed to the compound concentrations described above, had been recorded at the appropriate time points. Drug compounds were added as 100 μl volumes at 2X the desired concentration to each well of a 96-well low adhesion round bottom plate containing 100 μl of normal media and a single cardiac organoid, and allowed to incubate for 30 min at 37 °C. The plate was then recorded, 3 organoids at a time, using the process described above until all organoids were recorded and the plate was returned to the incubator. The process was then repeated 24 h and 48 h later. The 20 s videos were then analyzed; beats were counted for each video and multiplied by 3 to scale values to beats per minute. A beat was defined as the beginning of the contractile movement of the organoid; a beat did not need reach conclusion to be counted. If multiple beating regions were observed, then the beating of the largest multi-cell structure was used to calculate the beating rate. If all doses caused a cessation in beating, then a lower dose was added in order to find the lowest possible dose to significantly reduce beat rate.

2.7. Lung module fabrication

Lung modules were prepared as described previously [9]. Briefly, the 3D airway organoid constructs were modeled on the structure and cellular organization that are present in the airways. Specifically, a 3D multi-layered approach was employed within the context of the microfluidic device fabrication methodology described below. First, a polyester transwell membrane, typically immobilized within the microfluidic device, was coated with a lung-specific ECM derived from human donor lung tissue that was decellularized and processed as we have described previously for other tissue types [9, 10, 29]. Organoids were fabricated in three layers; Lower: lung microvasculature endothelial cells (Lonza CC-2527), Middle: airway stromal mesenchymal cells (donor derived), and Upper: bronchial epithelial cells (Lonza CC-2540S) cultured above the stroma (figure 5(g)). The layering approach rapidly produces a basic multicellular organization similar to that seen in native airway tissue, with an endothelium forming a vascular barrier exposed to liquid media, a stromal mesenchyme layer at the core of the 3D tissue structure, and a polarized airway epithelium exposed to the air interface to stimulate cell polarization and maturation. Cells were maintained in Clonetics™ B-ALI™ air-liquid interface medium growth medium for 48 h before performing air-lift and media change in the lower chamber with B-ALI™ differentiation medium. Media changes were performed every 48 h.

2.8. Vascular module fabrication and characterization

The vascular endothelium module, comprised of endothelial cells on a membrane, was created in a modified microreactor device, fitted to be compatible with the existing fluidic system hardware. Briefly, PDMS layers with circular windows cut using a 4 mm biopsy punch were used to sandwich a Transwell membrane (Corning) and sealed with a thin layer of PDMS. These components were cured at 80 °C for at least 90 min. A solid bottom layer and a top layer with inlet and outlet ports to integrate with the fluid circuit were clamped together with PMMA clamps. The membrane was sterilized with EtOH and coated with fibronectin prior to introduction of cells. Endothelial cells (HUVECs, 50 000 cells) were seeded on the membrane in EGM-10 media and allowed to attach overnight under static conditions.

Trans-endothelial electrical resistance (TEER) sensors were built in-house, as is described in figure S4. Briefly, electrodes with cylindrical gold probe heads (0.95 mm radius, 2 mm height) were fabricated into the endothelium module devices, with 5 mm spacing between electrodes. Measurements were documented from readings using a standard voltmeter (TekPower TP2844R) by connecting the probes to the 2 TEER electrodes, during which a function generator (GW Instek GFG-8216A), also connected to the electrodes, was employed to generate the electrical signal. The function generator was applied under the following parameters: Frequency—12.5 Hz; Amplitude—6.4 V; Waveform—Sine wave.

First, modules were cultured for 4 days, after which IHC and LIVE/DEAD staining were performed. For IHC, similar staining protocols as described above were performed using antibodies for CD31

(raised in mouse, cat. # M0832, Dako), von Willebrand Factor (raised in rabbit, cat. # AB7356, Millipore), and VE-Cadherin (raised in goat, cat. # sc-6458, Santa Cruz), and the appropriate Alexa Fluor 488 secondary antibody. Stained sections were imaged on a Leica upright microscope. LIVE/DEAD staining and imaging under macro-confocal microscopy was performed as described above.

For validation of TEER resistance levels during attainment of confluency, readings were taken once daily for 4 days (n = 3) using modules seeded with 50 000 HUVECs. In parallel, readings were taken using modules with no cells.

For the first endothelial response experiment, modules were prepared as described above, and readings were taken under normal conditions after confluency had been reached. Readings were then taken after addition of 100 μM histamine (Sigma) and 5 and 10 min following administration. Next, fresh EGM-10 was added, replacing the histamine-containing media, and readings were taken then and 5 min later.

To demonstrate the capability of the vascular endothelium to act as a barrier to mass transport between organoids, a hybrid liver-vascular module was fabricated. This module was comprised of the vascular device as described above, with the additional feature that liver organoids were immobilized in the lower chamber of the device below the endothelium.

For a measurable dye component, first a 15 kDa gelatin-based dye was prepared by tagging a thiol-modified gelatin with Alexa Fluor 594 maleimide. Briefly, 10 mg thiolated gelatin (Gelin-S, ESI-BIO) was dissolved in 500 μl sterile deionized water, after which the solution was diluted in EGM-10 to make 10 mL. Two μl Alexa Fluor 594 maleimide (1 μM in DMSO) was added to the gelatin solution and vortexed for 20 s. Under physiological pH or higher, thiol-maleimide reactions occur almost instantaneously, resulting in tagged soluble gelatin. The resulting dye-containing media was sterile filtered (0.45 μm filter, Millipore) and stored at 4 °C until use. A standard curve of dye-containing media was assessed for appropriate levels of fluorescent intensity on the plate reader prior to the endothelium dye transfer experiment.

To perform the experiment, 2 sets of endothelium modules were prepared (n = 3): one set consisted of confluent monolayers, and the second set consisted of non-confluent monolayers. Devices were assembled with liver organoids in the bottom chambers as describe above, with the gelatin dye-containing media having been mixed into the hydrogel solution. The devices, which were outfitted with inlet and outlet ports connected to a media reservoir/pump, and a sampling tube were immediately initiated under a flow rate of 25 μl min^{-1}. Sample aliquots were collected from the outlet tube every 5 min, providing volumes of approximately 125 μl for analysis. After 20 min, the inlet tube was shifted from the EGM-10-containing reservoir to a reservoir containing 100 μM histamine in EGM-10. Sampling continued at 5 min intervals until 45 min total time had elapsed. Aliquots (100 μl of the total 125 μl) were transferred to a 96-well plate, and fluorescent intensity was assessed using 584 nm for excitation and reading at 612 nm for emission on the plate reader.

2.9. Colon organoid formation and characterization

We received rabbit colonic smooth muscle cells (RCSMCs) from Dr Khalil Bitar (Wake Forest Institute for Regenerative Medicine, Winston-Salem, NC). These cells were isolated from fresh rabbit colons and purified through attachment to plastic. In addition, for the epithelial component, CACO-2 cells (ATCC.org, #HTB-37) were utilized. The cells were expanded in DMEM with 10% FBS and RCSMCs were discarded after 8 passages, as they lose the ability to remodel collagen. Cells were cultured on normal tissue culture plastic before being trypsinized (0.05% EDTA) when they reached the desired confluency. Collagen I (Corning) was prepared as per manufacturer's protocol; briefly, 600 ul of collagen I, 100 ul of PBS 10×, 14 ul of 1 N NaOH, and 286 ul of DMEM were mixed together to produce a neutralized solution of 2 mg ml^{-1} Collagen I. This solution was then further diluted with DMEM to produce a collagen solution with concentration of 0.5 mg ml^{-1}. RCSMCs were suspended in type I collagen at a density of 5 million cells/ml of collagen I and CACO-2 cells were suspended at a concentration of 500 000 cells ml^{-1}. Cell-collagen solutions were then deposited into custom made PDMS wells and allowed to culture for 3–5 days before immobilization in the microreactor.

Colon organoids were queried for morphology and cell surface marker expression by histological stains and immunofluorescent staining. Organoids were fixed, paraffin embedded and sectioned as described for other stains above. Overall organoid morphology was visualized by hematoxylin and eosin (H&E) staining. In particular, H&E-stained sections were assessed for organization of smooth muscle cells within the construct and the presence of epithelial acini structures formed by self-organization of the colon epithelial cells. Collagen fiber bundling and alignment was visualized by picrosirius red staining and imaging. Briefly, sections were stained with picrosirius red which dyes collagen fibers a deep red color. When imaged under polarized light, picrosirius stain produces a birefringent signal that shows bundled collagen in orange and reticular collagen in green. Lastly, sections were stained with antibodies for ZO-1, a cell-cell tight junction marker, and cytokeratin 18, a commonly employed marker for epithelial cells in the gut. For this IHC staining, the general IHC protocol described above was employed using primary ZO-1 (40-2300, ThermoFisher, raised in rabbit) or CK18 (ab82254, Abcam, raised in mouse) antibodies, followed by anti-rabbit and anti-mouse Alexa Fluor 594

secondary antibodies, respectively (ThermoFisher, raised in goat) for fluorescent visualization. DAPI was used to stain the nuclei of the cells.

2.10. Testis organoid formation and characterization

Testis organoids were comprised of primary spermatogonia, leydig, sertoli and peritubular myiod cells [30]. Adult testicular tissues (whole organ) from three brain dead patients (ages 56–61) were procured through the National Disease Research Interchange (NDRI). Spermatogonial stem cells (SSC), Leydig cells, and Sertoli cells were isolated from cryopreserved fragments of normal adult human testicular tissue. After isolation, Sertoli, and Leydig cells were immortalized using a lentivirus expressing hTERT to ensure prolonged propagation without changing their natural morphology and gene expression. Human SSC, Sertoli, and Leydig cells at passage 5–6 were re-suspended in testicular organoid formation media (complete StemPro-34, 30% FBS, 1 μg ml^{-1} solubilized human testis ECM at a ratio of 8:1:1 and seeded into 96-well format hanging drop plates (Perfecta3D, 3D Biomatrix, Ann Arbor, MI) at a density of 10 000 cells/40 μl drop volume. After 48 h, compact organoids were transferred into 96-well format ultra-low attachment U-bottom plates (Sigma-Aldrich, St. Louis, MO, USA).

Organoids were stained with hematoxylin and eosin for internal morphologic characterization. Drug effects were then analyzed on human testicular cells, either in 2D culture or in 3D organoid form. Cells were exposed to busulfan, cisplatin, doxorubicin, or etoposide in concentration ranges from 10^{-2} μM to 10^{3} μM for 48 h prior to determination of ATP content via CellTiter-Glo® Luminescent Cell Viability assays. Dose response curves were generated (n = 3). Following drug treatment, testicular organoid gene expression changes were assessed for key genes. Specifically, the fold-change (RelQ, 2-$\Delta\Delta$CT) for spermatogonia (PLZF (ZTBT16)), Leydig (CYP11A1, STAR) and Sertoli (SOX9) cell markers were measured to compare 3D testicular organoids to corresponding 2D testicular cell culture controls for the four clinically relevant chemotherapeutic drugs

2.11. Brain organoid formation and characterization

Brain organoids [31] contained six cell types. Specifically, organoids were comprised of approximately 2000 cells; 30% human brain microvasculature endothelial cells (HBMEC), 15% human brain vascular pericytes (HBVP), 15% human astrocytes (HA), 5% human microglia (HM), 15% human oligodendrocytes (HO), and 20% human neurons (HN). Organoids containing HA, HM, HO and HN were allowed to form in 50% astrocyte medium without astrocyte growth supplements and 50% neural maintenance-XF medium under normal growth conditions for 48 h in hanging drop culture plates (InSphero AG, Schlieren, Switzerland). The medium was mixed with heat inactivated FBS (ThermoFisher) and 10 ng μl^{-1} rat tail collagen I (Corning). HBMEC and HBVP were subsequently added to coat the neural-glial organoid. The organoids were cultured under normal growth conditions in 60% neural maintenance-XF medium (Axol Biosciences Ltd, Cambridge, UK), 20% astrocyte medium (ScienCell Research Laboratories, Carlsbad, CA) and 20% complete classic medium (Cell Systems, Kirkland, WA). The organoids were then allowed to mature further for 48 hr and were transferred into a 96-well plate for long-term use.

LIVE/DEAD staining (ThermoFisher) was used to evaluate cell viability as described above. The organoids were then imaged using an Olympus Fluoview Fv10i (Olympus, Tokyo, Japan) laser scanning confocal microscope.

Organoids were fixed in 4% formaldehyde (Polysciences Inc., Warrington, PA) for 15 min at 4 °C, permeabilized with 0.1% Tween-20 in PBS for 10 min at 4 °C, blocked using Protein Block (Dako Group, Troy, MI) for 1 hr at RT, and were subsequently incubated at 4 °C overnight in Antibody Diluent (Dako) solution containing primary antibodies –anti-O4 (a marker for oligodendrocyte precursor cells (OPC), 1:200, RD Systems), anti-Myelin Binding Protein (a marker for mature oligodendrocytes, 1:250, Millipore, Billerica, MA), anti-PDGFR-b [CD140b] (a marker for pericytes, 1:500, Millipore), anti-GFAP (a marker for astrocytes, 1:500, Millipore), anti-CD31 (a marker for endothelial cells, 1:1000, Abcam), anti-Iba1 (a marker for microglia 1:500, Abcam), anti-beta Catenin (1:500, Abcam), anti-MDR-1 (1:500, Millipore), anti-ZO-1 (1:1000, Millipore), anti-Claudin-5 (1:500, Millipore). Organoids were subsequently washed three times and incubated with Alexa Fluor 488 Goat anti-Mouse IgG (1:1000, ThermoFisher), Alexa Fluor 594 Goat anti-Rabbit IgG (1:1000, ThermoFisher), or Alexa Fluor 488 Goat anti-Chicken IgG (1:500, ThermoFisher) in Antibody diluent (Dako) overnight at 4 °C. Nuclear staining was performed by incubating the organoids with DAPI (1:1000) in PBS for 10 min. The organoids were washed and imaged using the Olympus Fluoview Fv10i (Olympus) laser scanning confocal microscope. At least three randomly selected organoids were imaged for each stain.

2.12. Microfluidic device fabrication

The microfluidic system design employed eliminates the use of PDMS as a substrate that can be exposed to media, thereby reducing chances for surface adsorption and subsequent absorption of drug compounds, toxins, soluble proteins, and secreted compounds onto/into the device walls. The device fabrication strategy is based on adhesive film microfluidics and laser cut poly(methyl methacrylate) (PMMA) components for manufacturing the device. The system

consists of seven layers; a glass layer, three double sided tape (DST) layers (3 M 9495MP, Minneapolis, MN), two PMMA layers and a Isopore 0.8 um TETP membrane (Cork, IR). These layers are partitioned into three functional layers, lid layer, chamber layer, microfluidics layer and membrane layer. All of the layers are fabricated with a laser cutter (Hobby Series 20 × 12 CO2 Laser Cutter, Las Vegas, NV). The lid layer consists of 1.8 mm holes for the inlet and outlet tubing in a 1 mm thick PMMA sheet. The chamber layer has the same patterned holes plus a 6-mm diameter chamber for the liver, heart, brain and testes tissue construct; plus 3 mm diameter chambers for the lung and blood vessel (BV). This layer is made out of a 3 mm PMMA sheet. attached to 100 μm DST on the top part. The microfluidic layer is patterned in two separated 100 μm DST sheets, the bottom layer without connectivity between lung and BV and the top one with it. In between the two fluidic sheets a porous membrane is placed for the corresponding constructs. Finally, everything is assembled onto the glass slide. All the layers are stacked, bound by DST, sealed after organoid integration, and Teflon tubing (Cole-Parmer, Vernon Hills, IL) is inserted in the appropriate inlet/outlets to connect the device to the pumped fluid circuit. A PDMS top layer with corresponding inlet/outlets provides the necessary seamless compression and mechanical stability minimizing leaking and the need for adhesives such as epoxy to seal tubing/port interfaces.

2.13. Multi-organoid integration and culture

Each type of tissue organoid or construct was prepared as described above and introduced to devices described above. In each system, the following preparation steps were performed in each organoid chamber to represent *in vivo* ratios of tissue volumes where possible. Fifty liver organoids were immobilized within a 50 μl volume of a liver-ECM supplemented hyaluronic acid (HA) and gelatin hydrogel (HyStem-HP, ESI-BIO, Alameida, CA) [9, 10, 29]. Ten cardiac organoids were immobilized in 25 μl fibrin hydrogel (Sigma) [9]. Two testicular organoids were immobilized in 25 μl HA and gelatin hydrogel. Brain organoids were immobilized in 25 μl HA and gelatin hydrogel. Vascular and lung modules were initiated on chip as described above. Five colon constructs were prepared as described above and immobilized in 50 μl HA and gelatin hydrogel. The device was then sealed with the top layer of PMMA containing inlet and outlet tubing and connected to the micro-peristaltic pump (Elemental Scientific, Omaha, NE) and media reservoir. The media reservoir was filled with 5 mL of the common media formulation, which consisted of testis organoid media and EGM media (with supplements, but without FBS) mixed in a 1:1 ratio by volume. Flow was initiated at 10 μl min^{-1}. Six systems were initiated for the study, with three systems sacrificed on day 7 for viability assessment by LIVE/DEAD staining and macro-confocal microscopy imaging. The remaining systems were sacrificed on day 15 for the same assessment. During the experimental time course media aliquots were removed for soluble biomarker analysis on day 4, day 7, day 11, and day 14. Aliquots were frozen and stored at −80 °C until the panel of ELISAs and colorimentric assays were performed. ELISAs were employed to measure albumin (Alpha Diagnostics International), creatine kinase (Abcam), interleukin-8 (Abcam), and prostacyclin (Abcam). Colorimetric assays were employed to measure urea (BioAssay Systems) and lactate dehydrogenase (Invitrogen).

2.14. Integrated drug response

Six-tissue platforms were initiated (six systems in total) containing liver, cardiac, lung, vascular, testis, and brain organoids, as described above, and maintained for 7 days prior to the start of the drug study. At this point, the liver modules were removed from half of the platforms ($\mathbf{n = 3}$). Capecitabine, the chemotherapy prodrug to 5-fluorouracil (20 μM, Sigma), was administered to all platforms after which viability was assessed through LIVE/DEAD staining after 7 days of exposure. Next this study was repeated using cyclophosphamide, an alkylating chemotherapy prodrug (20 μM, Sigma), in 5-organoid systems containing liver, cardiac, lung, vascular, and testis constructs. Viability was assessed on day 14 through LIVE/DEAD staining after 7 days of exposure.

2.15. Statistical analysis

The data are generally presented as the means of number of replicates ± the standard deviation. All data are graphed and analyzed for significance using a Student's T-test. For ATP activity assays p-values were considered significant under 0.01. For beating kinetic assays p-values were considered significant under 0.05. Data samples were eliminated from the experimental groups if they fell outside of two standard deviations from the experimental group averages.

3. Results

3.1. FDA-recalled drugs induce toxicity in 3D human organoids and differ from 2D cultures

To demonstrate the utility of 3D bioengineered human organoids, the responses to a panel of drugs that had been recalled from the market for causing either liver or cardiac toxicity were determined. Three of these recalled drugs were shown to cause toxicity in the liver: bromfenac, tienilic acid, and troglitazone (table S1 is available online at stacks.iop.org/BF/12/025017/mmedia). Seven drugs were screened that caused toxicity in the heart: astemizole, cisapride,

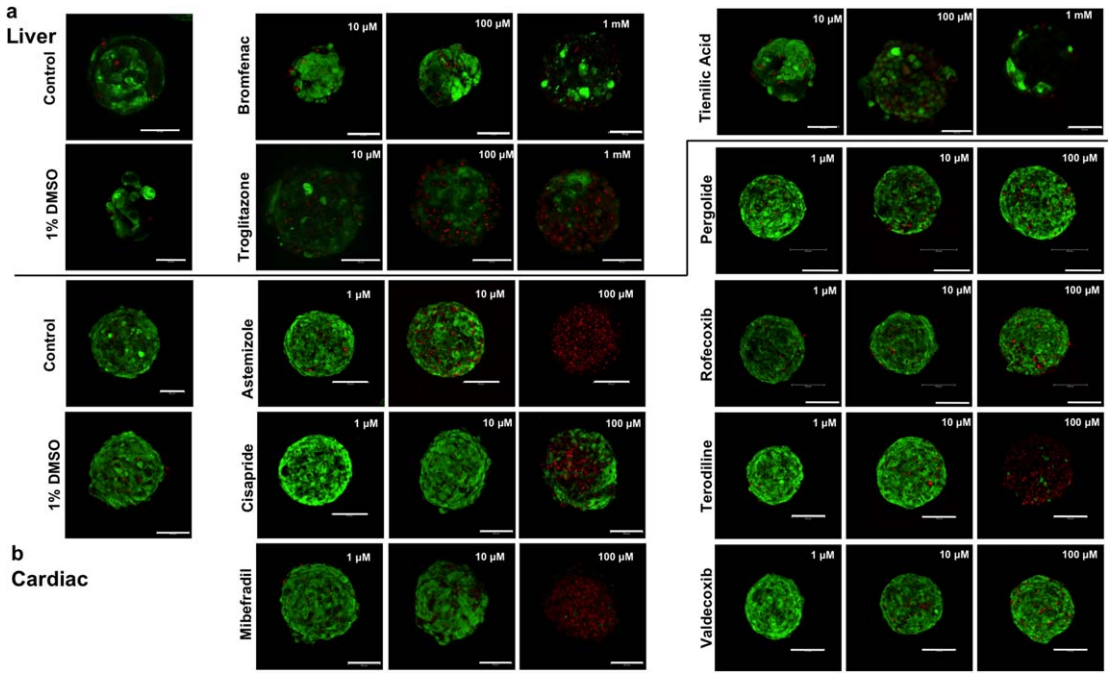

Figure 1. Compilation of LIVE/DEAD images as an effect of screened recalled drug compounds. (a) Liver organoids under control conditions, 1% DMSO, and varying concentrations of bromfenac, troglitazone, and tienilic acid. (b) Cardiac organoids under control conditions, 1% DMSO, and varying concentrations of astemizole, cisapride, mibefradil, pergoglide, rofecoxib, terodeline, and valdecoxib. Green—calcein AM-stained viable cells; Red—ethidium homodimer-stained dead cells. Scale bar—100 μm.

mibefradil, pergolide, rofecoxib terodiline and valdecoxib (table S1).

Liver or cardiac organoids were exposed to concentrations of these compounds ranging from 1 nM to 100 μM, for 48 h. In parallel, studies were performed for the same length of time using commonly used cells for drug modeling in 2D; specifically, primary hepatocytes or iPSC-derived cardiomyocytes, and liver HepG2 or heart C2C12 myoblast cell lines. Drug toxicity was measured using LIVE/DEAD viability/cytotoxicity staining and quantification of ATP activity. For cardiac organoids, beat rates were also assessed.

LIVE/DEAD staining of organoids was used to visualize acute toxicity in tissue organoids (figure 1). Quantification of these stains is presented in figure S1. These assays report on cellular death as opposed to impairment of function. Vehicle control live/dead images in cardiac and liver exposed to 1% DMSO showed no signs of cellular toxicity. Bromfenac toxicity is noted at 100 μM and with significant toxicity seen at 1 mM. Tienilic acid toxicity is first apparent at 100 μM, with cellular disorganization and cellular death being noted. Very few cells remained alive at 1 mM. Troglitazone induced cell death is significant at 100 μM and this toxicity is increased at 1 mM. Astemizole toxicity is noted at 10 μM, and at 100 μM the entire organoid is dead. Cisapride toxicity appears at 10 μM, and at 100 μM a large section of the organoid is dead. Mibefradil toxicity occurs at 10 μM and at 100 μM the entire organoid is dead. Terodiline toxicity is noted at 10 μM with many cells dead and at 100 μM the vast majority of cells within the organoid have died. Pergolide, rofecoxib, and valdecoxib did not cause severe cell death in doses below 100 μM, however, sporadic cell death was observed across all three recalled drugs at 100 μM.

ATP activity tests ($\mathbf{n \geqslant 6}$) were utilized in order to mimic large-scale drug screens over a logarithmic scale of doses. Bromfenac showed a significant loss of ATP at 1 mM (figure 2(a)). Tienilic showed significant loss of ATP at 1 mM ($P < 0.05$) (figure 2(b)). Troglitazone began a downward trend at 100 μM, reaching a significant p-value at 1 mM (figure 2(c)).

Of the seven cardiotoxic drugs tested for ATP reduction, four reached an IC50 value (Astemizole, Cisapride, Mibefradil and Terodiline) with the other three not producing significant toxicity over the initial range of doses (Pergolide, Rofecoxib, Valdecoxib). However, these three drugs did demonstrate a loss of ATP at 1 mM. Astemizole reached IC50 between 1 μM and 10 μM and reached significant loss at 10 μM (figure 2(d)). Cisapride reached the IC_{50} between 10 uM and 100 uM and showed significant ATP loss at 10 μM (figure 2(e)). Mibefradil IC_{50} was reached between 10–100 μM with significant ATP loss at 10 μM (figure 2(f)). Pergolide did not reach an IC_{50} until 1 mM but did reach a significant p-value at 100 μM (figure 2(g)). Terodiline reached an IC_{50} value between 10 μM and 100 μM and demonstrated a significant loss of ATP at 100uM (figure 2(h)). Rofecoxib reached an IC_{50} at 1 mM with significant loss measured at this same concentration. Valdecoxib did not reach an IC_{50} until 1 mM but did show significant loss of ATP at 100 μM (figure 2(i)).

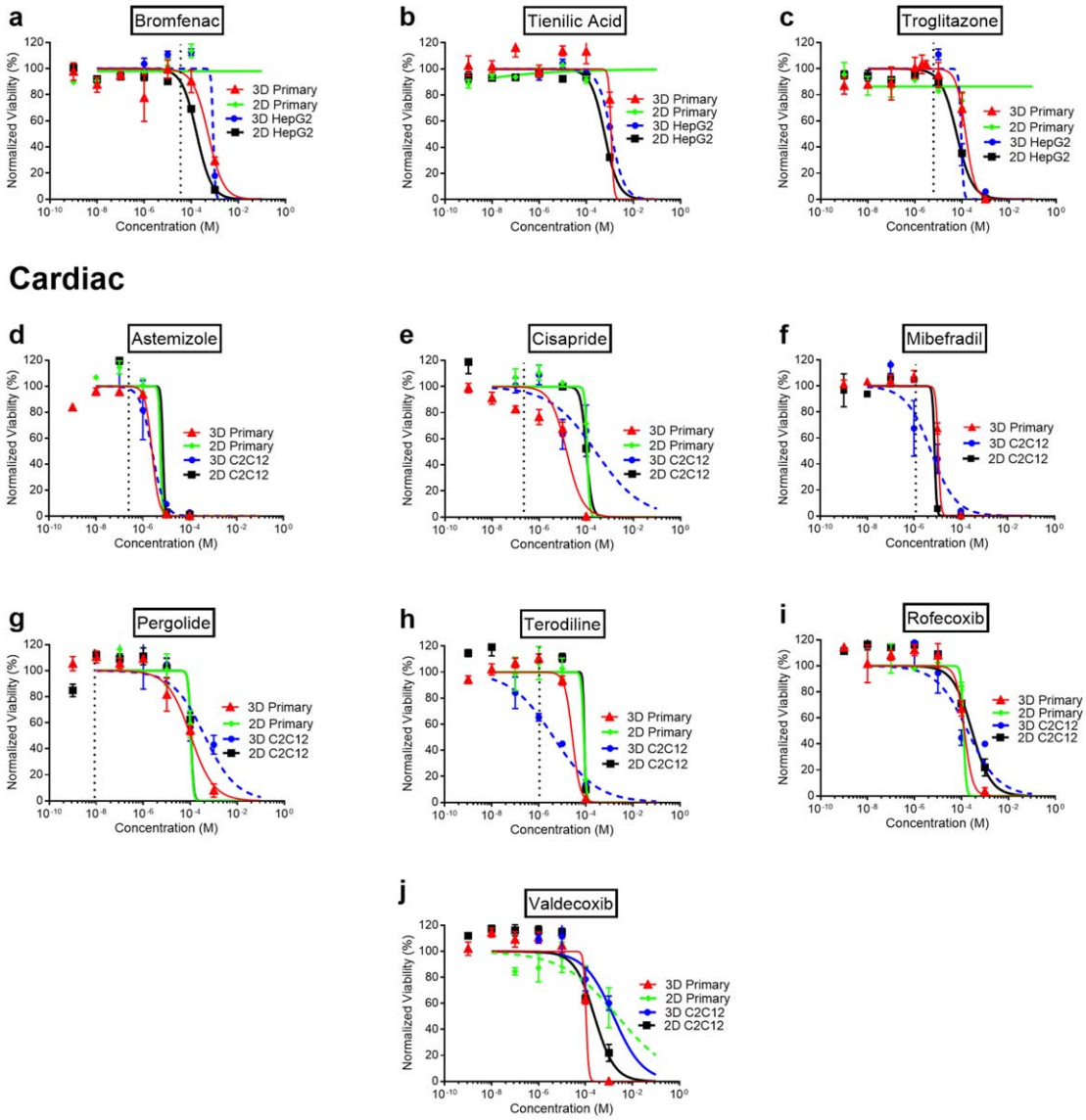

Figure 2. ATP activity in response to recalled drug compounds. ATP response in IC_{50} curve format for 3D primary human liver organoids in comparison to primary human hepatocytes in 2D culture and HepG2 hepatoma cells in 3D spheroids or 2D culture under exposure to (a) bromfenac, (b) tienilic acid, and (c) troglitazone. ATP response in IC_{50} curve format for 3D cardiac organoids in comparison to cardiomyocytes in 2D culture and C2C12 myoblasts in 3D spheroids or 2D culture under exposure to (d) astemizole, (e) cisapride, (f) mibefradil, (g) pergoglide, (h) terodiline, (i) rofecoxib, and (j) valdecoxib.

While liver toxicity manifests in cell damage and death, cardiotoxicity typically does not. Rather, cardiotoxicity takes the form of changes in the beat kinetics of cardiomyocytes. As such, beat rates of cardiac organoids were assessed at multiple time points over a range of drug concentrations. Rates of cardiac beating were affected by four of the seven recalled drugs in the original dose range (1 nM–100 μM) tested: Astemizole, Cisapride, Mibefradil, and Terodiline; while the other three, Pergolide, Rofecoxib and Valdecoxib, displayeding beat cessation at the 1 mM dose (figure above). Astemizole showed the largest effect on beat rate at two days, with all doses tested affecting this rate. A dose of 100 nM affected the beat rate at 30 min (figure 3(a)). Cisapride affected the beat rate at 1 μM after only 30 min. At two days, a 100 nM dose caused cessation of beating in one organoid (figure 3(b)). Mibefradil caused reduction of beat rate at 100 μM after 30 min and at 1 μM after two days. At 1 μM, one organoid ceased beating and at 10 μM, two stopped. With an number of 6, this did not produce a significant p-value but should be noted (figure 3(c)). Pergolide displayed no observable effects for the original doses tested. However, at 1 mM Pergolide induced a reduction in beat rate after two days. Similarly, rofecoxib displayed a reduction in beat rate at 1 mM after only 30 min (figure 3(d)). Terodiline showed effective depression of beat rate at 10 μM after 30 min (figure 3(e)). Rofecoxib effected beat rate at 30 min (figure 3(f)). Valdecoxib showed reduction in beat rate

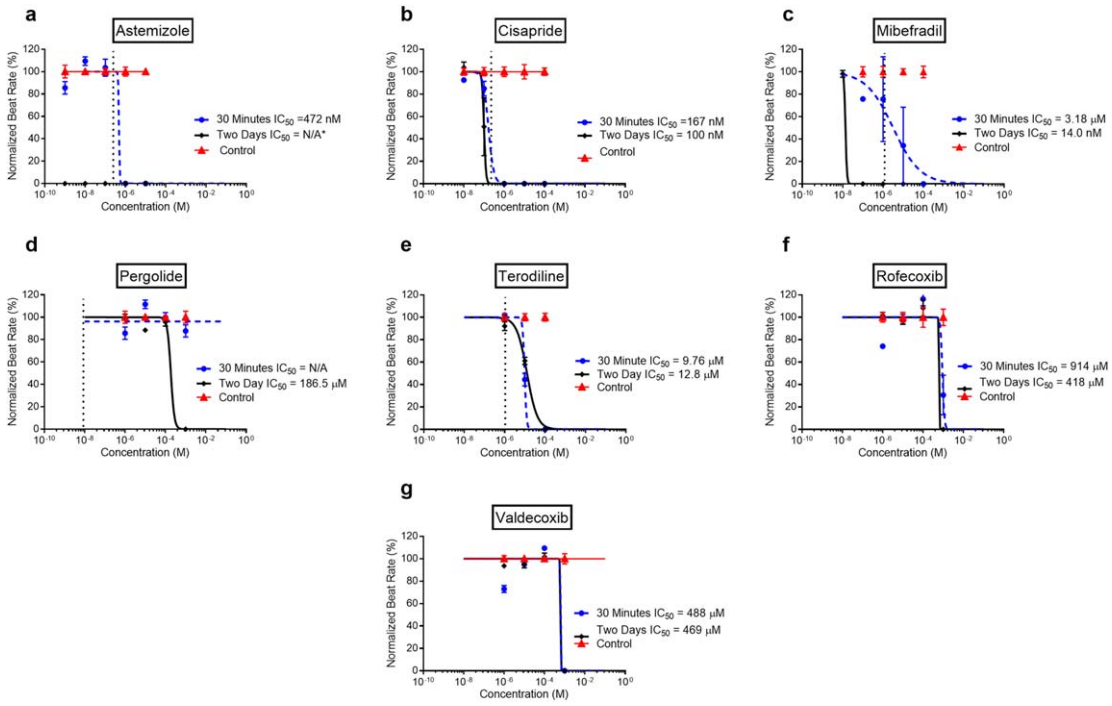

Figure 3. Cardiac organoid beating rate changes in response to recalled drug compounds. Beating rates were quantified as an effect of a range of drug concentrations after 30 min exposure, 48 h exposure, and no drug (control). Drugs screened included (a) astemizole, (b) cisapride, (c) mibefradil, (d) pergoglide, (e) terodiline, (f) rofecoxib, and (g) valdecoxib.

at the 1 mM dose (figure 3(g)). Summarization of these drug study data are presented in table S2. Additional morphological and visual observations are also described in figure S2. Importantly, we compared IC_{50} values in the organoids, both for ATP, and in the case of cardiac organoids the beating rate data, or LIVE/DEAD images, to observed toxic clinical plasma levels, which are summarized in table S3 [32–44]. Some toxic clinical plasma levels in patients were difficult to calculate from the literature (rofecoxib, valdecoxib, and tienilic acid), but by in large toxic clinical plasma levels were within one order of magnitude of concentrations that resulted in toxicity in the organoids (table S2). It should be noted that for the few drugs where IC_{50} values were high or not reached (bromfenac and tienilic acid), these likely require significantly longer exposures akin to the treatment durations in patients required for toxicity to manifest.

Traditionally, 2D cell cultures have been the standard for toxicity screening in drug development studies, but these may not fully recapitulate *in vivo* biology [45–50]. Because of their widespread use, we compared the effects of these drugs on liver and cardiac organoids with 2D cultures of primary human hepatocytes and HepG2 hepatoma cells used to screen for hepatotoxicity, and iPSC-derived cardiomyocytes and C2C12 myoblasts used to test for cardiotoxicity. In addition, spheroids of HepG2 and C2Cl2 cells were also employed as comparisons (figures 2(a)–(i)). Effective concentrations for inducing a decrease in ATP were often lower in the 3D organoids, as compared to both 2D primary cells, 2D cell lines, and cell line spheroids. Cells in 2D often displayed a higher degree of variability, leading to lower result significance; with this occurring most notably in 2D cardiomyocytes and C2C12 cells. It is interesting that in some cases 3D organoids were more sensitive to compounds, while in other cases 3D organoids were more drug resistant to toxic effects. Despite the lack of a clear trend, these discrepancies speak to the need to better understand how cell cultures and organoids respond to drugs and which models best reflect responses in humans. Moreover, these results underscore the use of organoid systems as being complementary to existing methods in order maximize the detection of unsafe compounds before they reach the clinic.

3.2. Over the counter compounds fail to cause organoid toxicity

To further test these organoids for clinical accuracy, we performed additional sets of screening studies with compounds generally considered non-toxic in humans. Specifically, we exposed liver and cardiac organoids to the common over-the counter drugs or supplements aspirin (NSAID), ibuprofen (NSAID), ascorbic acid (vitamin C), loratadine (anti-histamine), and quercetin (plant flavanol supplement) for 48 h using concentration ranges from 1 μM to 1 mM. Outcomes were assessed as described above, employing LIVE/DEAD staining, ATP activity quantification, and cardiac organoid beating rate quantification. LIVE/DEAD staining of liver organoids (figures S3(a)–(f)) showed virtually no observable cell death, with the exception of loratadine and quercetin at

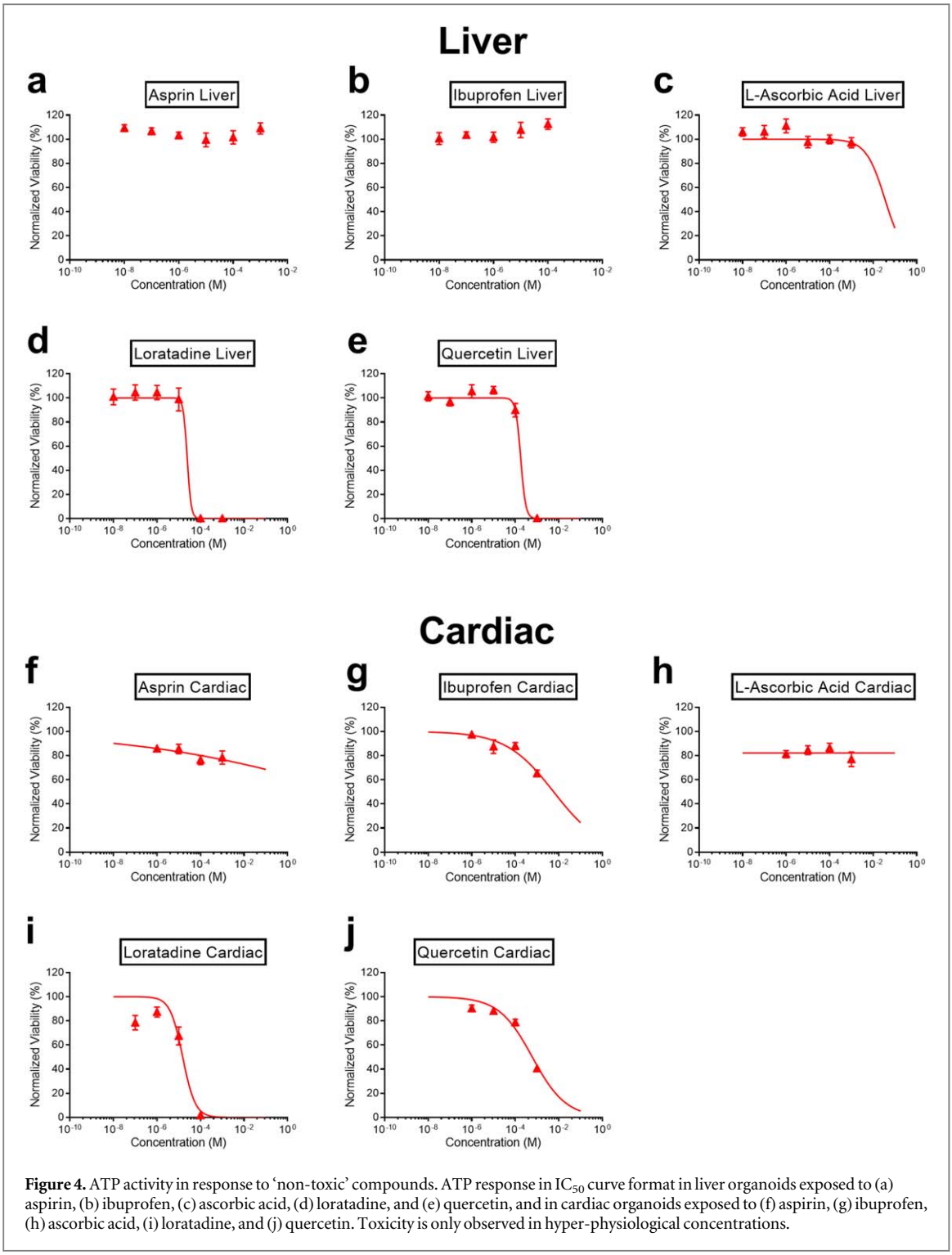

Figure 4. ATP activity in response to 'non-toxic' compounds. ATP response in IC_{50} curve format in liver organoids exposed to (a) aspirin, (b) ibuprofen, (c) ascorbic acid, (d) loratadine, and (e) quercetin, and in cardiac organoids exposed to (f) aspirin, (g) ibuprofen, (h) ascorbic acid, (i) loratadine, and (j) quercetin. Toxicity is only observed in hyper-physiological concentrations.

concentrations significantly higher than plasma levels in human subjects (2–3 nM and 0.5 μM, respectively) [51, 52]. Similar outcomes were observed in cardiac organoids (figures S3(g)–(l)), with the addition of some observable cell death as an effect of 1 mM aspirin, which is also significantly higher than typical plasma levels in human subjects taking aspirin (1-3 nM) [53]. Quantification of these data is presented in figure S4. These LIVE/DEAD viability data are echoed by ATP activity quantification (figure 4), which show complete lack of ATP decrease in liver and cardiac organoids until the high concentrations described above. Lastly, beating rates of cardiac organoids were determined after 30 min and 48 h exposure to the compounds (figure S5). Aspirin, ibuprofen, and ascorbic acid exposure resulted in negligible changes in beat rates, while loratadine and quercetin did result in decreased beating rates, but only at the high concentrations described above, which were significantly higher than normal plasma levels in humans taking the drugs. Based on these data, and those described above, we believe that these organoids consistently

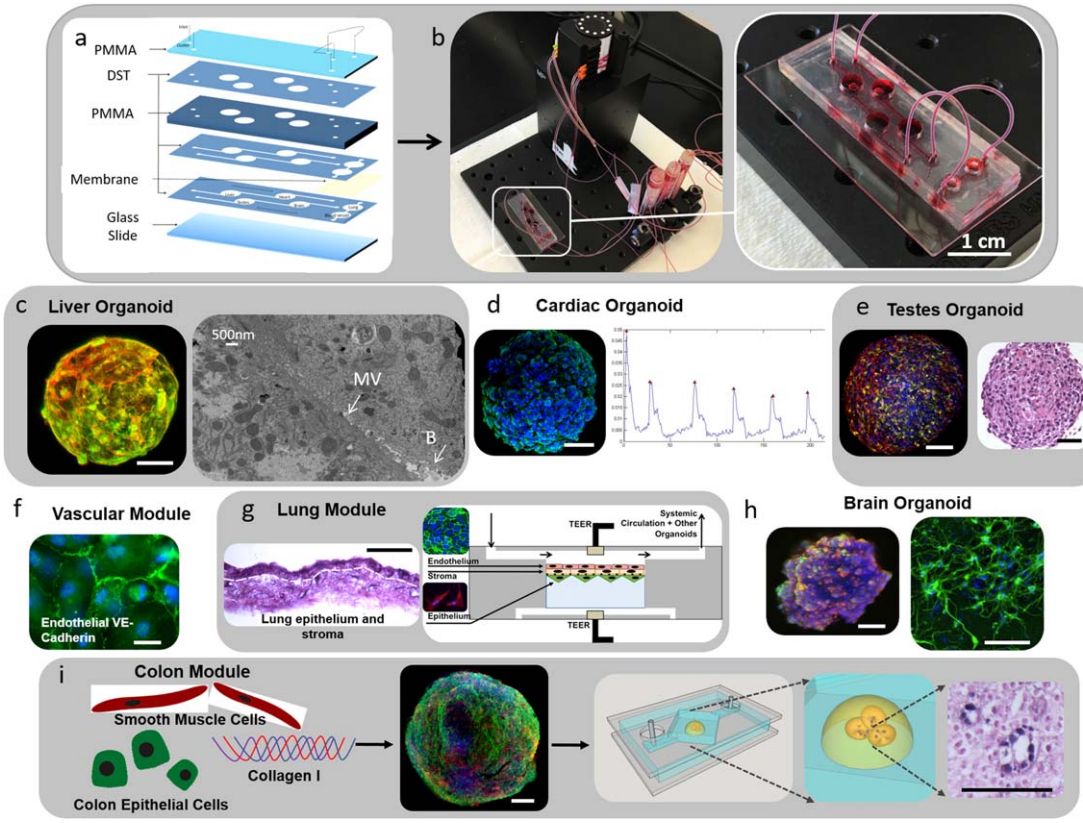

Figure 5. Visual overview of the multi-organoid platform. (a) Microfluidic devices are fabricated in a PDMS-free approach by layering PMMA and adhesive films with chambers, channels, and ports formed by laser cutting. Organoids are incorporated by being immobilized in hydrogels within each chamber. Semi-porous membranes enable inclusion of planar vascular and lung modules. (b) A fabricated 6-tissue device under fluid flow provided by a micro-peristaltic pump and media reservoir. The total device footprint is 7.0 by 2.4 cm, or roughly the size of a traditional microscope slide. (c) Liver organoids are comprised of human hepatocytes, stellate cells, and Kupffer cells and feature internal microstructures such as hepatic microvilli (MV) and bile caniculi-like structures (B). (d) Cardiac organoids are comprised of iPSC-derived cardiomyocytes and cardiac fibroblasts and beat spontaneously. (e) Testicular organoids are comprised of spermatogonial stem cells, Sertoli, Leydig and peritubular cells. (f) Vascular and (g) lung modules are comprised of planar cellular layers supported by a semi-permeable membrane. (h) Brain organoids are comprised of human brain microvascular endothelial cells, neurons, oligodendrocytes, microglia, pericytes, and astrocytes. (i) Colon modules are comprised of colon smooth muscle cells that form an aligned matrix environment in which colon epithelial cells exist as acini. Scale bars, unless otherwise noted in the figure, scale bars are 100 μm; except (f) and (h) (right panel), which are 50 μm.

recapitulate responses to both toxic and non-toxic drug compounds under acute exposures. Additional work will be performed to expand investigation into chronic drug exposures.

3.3. Six-organoid integrated platform

Ultimately, because tissues and organs do not exist in isolation, *in vivo*, bioengineered organoid systems should contain representations of several tissue types under a common medium. This would best model tissues and organs in the body under a common blood supply. One goal of the current project was to build upon our previously described 3-organoid platform [9] to develop a functional 6-tissue body-on-a-chip system, containing representations of liver, heart, vasculature, lung, testis, and either colon or brain (figure 5(a)). Importantly, these individual tissue types would be constructed in an integrated microfluidic hardware platform (figure 5(b)), formed by laser cut poly(methyl methacrylate) (PMMA) and adhesive films, rather than conventional polydimethyl-siloxane (PDMS) soft lithography and molding [54, 55]. This was intended to avoid absorption of proteins and drug compounds into the device walls—a significant problem with PDMS [56]. Because of the specific individual requirements of each type of tissue organoid, a toolbox of biofabrication techniques was employed to create each tissue model. Briefly, using non-adherent round-bottom 96-well plates, spherical liver organoids (figure 5(c)) were formed with primary human hepatocytes, stellate cells, Kupffer cells, and endothelial cells. Spherical cardiac organoids (figure 5(d)) were formed using iPS-derived cardiomyocytes, endothelial cells, and cardiac fibroblasts. Testis organoids were formed using primary spermatogonia, leydig, sertoli and peritubular myeloid cells (figure 5(e)) [30]. These spherical organoids were then incorporated into the microfluidic devices using a liver ECM-derived bioink, a fibrin and gelatin bioink, or a hyaluronic acid and gelatin bioink, respectively; employing crosslinking of the hydrogel bioinks to immobilize the organoids as larger hydrogel-organoid constructs within the

perfusion system. Vascular (figure 5(f)) and lung modules (figure 5(g)) were fabricated in a different form factor, using semi-porous membranes immobilized within the devices on which human umbilical vein endothelial cells (vascular) or lung fibroblasts, lung epithelial cells, and lung endothelial cells were seeded. A custom-built trans-endothelial electrical resistance (TEER) sensor was employed, which was integrated into the endothelium module device itself. This sensor measures the electrical resistance across the endothelium using 2 gold electrodes on either side of the monolayer, allowing monitoring of endothelial or epithelial barrier integrity. Brain organoids (figure 5(h)) were formed as spherical structures using primary human brain microvascular endothelial cells, human brain vascular pericytes, human astrocytes, human microglia, human oligodendrocyte precursor cells, and iPSC-derived neurons [31]. Lastly, colon organoids (figure 5(i)) were formed by molding collagen Type I gels with colon smooth muscle cells [57] and epithelial cells, resulting in aligned collagen submucosal tissue containing epithelial acini structures. Following biofabrication, devices were sealed and connected to the circulatory perfusion system with a common media driven by a micro-peristaltic pump.

Extensive individual tissue model characterization data for liver, cardiac, and lung has been described previously [9, 29, 58, 59], including histology, immunostaining, metabolic assays, basic drug toxicity testing, and additional functional tests, demonstrating the physiological relevancy of each tissue model type. For the recently added tissues, characterization studies were performed to verify viability and function of the vascular module (figure S6), colon (figure S7), testis (figure S8), and brain organoids (figure S9) (materials and methods and supplementary materials).

3.4. Integration of multiple organoid types results in a steady state, highly viable platform

Our first goal in using the 6-tissue system was to assess the stability of the system over time under baseline conditions. The platform described above was assembled and equilibrated under circulating perfusion at 10 μl min^{-1}. The common media contained a 1:1 mix of serum-free endothelial cell media and testicular cell media. Viability was shown for 28 days, visualized at days 7, 14, and 28 by LIVE/DEAD staining and imaging by macro-confocal microscopy (figures 6(a), (b)) Interestingly, a panel of secreted biomarkers (figures 6(d)–(i)) indicate an initial increase in inflammatory markers that returns to baseline after a week. Throughout the study, other markers of toxicity remain low with functional markers remaining consistently expressed. Specifically, baseline liver function (albumin and urea) remains constant and significantly higher than media controls for the duration of the study; indicating maintenance of viability and function (figures 6(d)–(e)). Likewise, lactate dehydrogenase (LDH), a general marker of toxicity for all tissue types, and creatine kinase (CK), a marker of toxicity in cardiomyocytes, remained low—at similar levels to the media controls (figures 6(f)–(g)). Interestingly, IL-8 and prostacyclin, proteins released from lung epithelium and vascular endothelium, respectively, initially spike, but decrease to baseline over time, suggesting that the lung and vascular constructs experienced stress upon system initiation, but improve over time (figures 6(h)–(i)). These data suggest that the multi-organoid system self-regulates, conditioning the media over time to better support each tissue type in a manner perhaps similar to the human body.

3.5. Integrated drug study reveals inter-organoid drug dependence

As demonstrated previously [9], integration of multiple organoids within a common recirculating media environment enables more complex, and more physiologically relevant drug studies to be performed. This is because one or more organoids can respond to an administered compound in ways that influence other organoids in the system. Here we further explore this concept using 6- and 5-organoid platforms, in which system dependency on liver organoid metabolism is demonstrated. Microfluidic platforms were fabricated as described above and cultures were initiated as 6-organoid systems containing liver, cardiac, lung, endothelial, testis, and brain organoids or as 5-organoid systems containing the same organoids above, but without brain organoids. These systems were maintained for 7 days prior to the initiation of the studies. At this point, the liver modules were removed from half of the platforms. Capecitabine (20 μM) was administered to all 6-organoid platforms while cyclophosphamide (20 μM) was administered to all 5-organoid platforms. Viability was assessed through LIVE/DEAD staining after 7 days of exposure (day 14 of total study). These drugs are notable in that they are pro-drugs that have been used to treat cancer. As such, they require metabolism in the liver to be processed into active metabolites. This is conceptually described in figure 7(a), where in panel (i), without the liver present, the drug cannot be metabolized into its active form. As a result, there is no reduction in cell viability, as the toxic metabolite is not present. Conversely, in panel (ii), when the liver organoid is present, the pro-drug is metabolized into its active form, causing cytotoxicity in several downstream organoids. Macro-confocal microscopy imaging of LIVE/DEAD stained organoids showed the anticipated results. Following exposure to capecitabine, systems without liver organoids do not show significant toxicity in any downstream organoids. However, systems containing liver were able to metabolize the capecitabine into 5-FU, and toxicity was observed in the cardiac and lung

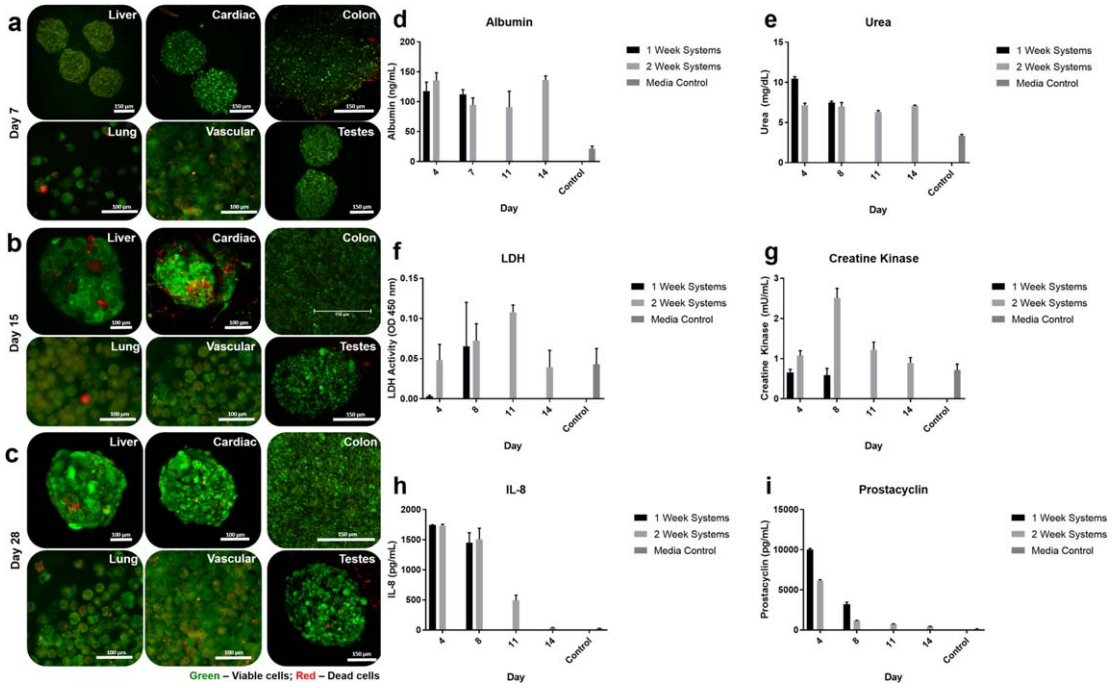

Figure 6. Six organoid maintenance under a common media the body-on-a-chip system. (a) 7-day, (b) 14-day, and (c) 28-day viability of liver, cardiac, colon, lung, vascular, and testis tissue models in the integrated system. Green—Calcein AM-stained viable cells; Red—Ethidium homodimer-stained dead cells. C-H) Biomarkers in solution show that the system reaches an apparent equilibrium state. (d), (e) Albumin and urea quantification shows relatively consistent secreted albumin and urea in the media over time, that is significantly higher than media controls. (f) LDH, a general marker of lysed cells and toxicity, remains at levels near that of media controls, indicating relatively low cell death. (g) Creatine kinase, a biomarker released by lysed cardiomyocytes upon cell death remains relatively low, with the exception of a spike on day 8 that returns quickly to a concentration near media control levels. (h), (i) IL-8 and prostacyclin, proteins released from lung epithelium and vascular endothelium, respectively, initially increase, but decrease to baseline levels over time, suggesting that the lung and vascular constructs experienced stress upon system initiation, but equilibrate to a steady state over time.

organoids (figure 7(b)). In the experiment using cyclophosphamide, systems without liver organoids did not metabolize the prodrug to an active form, and no toxicity was observed. Conversely, with liver organoids present, metabolism of the compound into a toxic metabolite resulted in toxicity in both the cardiac and lung constructs (figure 7(c)). Quantification of these LIVE/DEAD data are presented in figure S10.

4. Discussion

Development of new drugs has been slow and expensive, due in part to limitations of current *in vitro* and *in vivo* drug screening models. Traditional, 2D cell cultures do not fully recapitulate the 3D cellular microenvironment of normal human tissues [6–8]. By supplementing current testing methods with 3D systems such as tissue organoids, many of these shortcomings may be overcome. Organoids have the capability to respond to drugs and toxins in much the same manner as actual human organs, and as such, may provide an improved platform for drug screening applications. Furthermore, recent advances in tissue chip devices and tissue organoid integration [24, 60] provide additional capabilities that take into consideration the complex interactions that can occur among different organs and tissues types.

In the work presented here, two major accomplishments are described. First, 3D primary human liver organoids and 3D iPSC-derived cardiac organoids were employed to screen a panel of drug compounds that were withdrawn from the market for causing liver and cardiac toxicity in human subjects. These compounds were tested by the pharmaceutical industry and toxicity was not noted using standard 2D cell culture systems, rodent models, and during human Phase I, II and III clinical trials. However, after the drugs were released to market and administered to larger numbers of patients, toxicity was noted causing the FDA to withdraw regulatory approval. In most all of these compounds, the 3D organoid system was able to readily demonstrate toxicity at a human relevant dose. Bromfenac was an NSAID intended for pain relief following opthalamic surgery and was recalled due to hepatotoxcity [61]. Tienilic acid was a uric acid lowering diuretic for the treatment of hypertension that was recalled after it was discovered to be a suicide inhibitor of cytochrome P450, causing hepatotoxicity [62–64]. Troglitazone was an anti-inflammatory treatment involved in downregulating the NFK-B pathway for type 2 diabetes and was recalled after causing liver failure in dozens of patients [65, 66]. Astemizole was

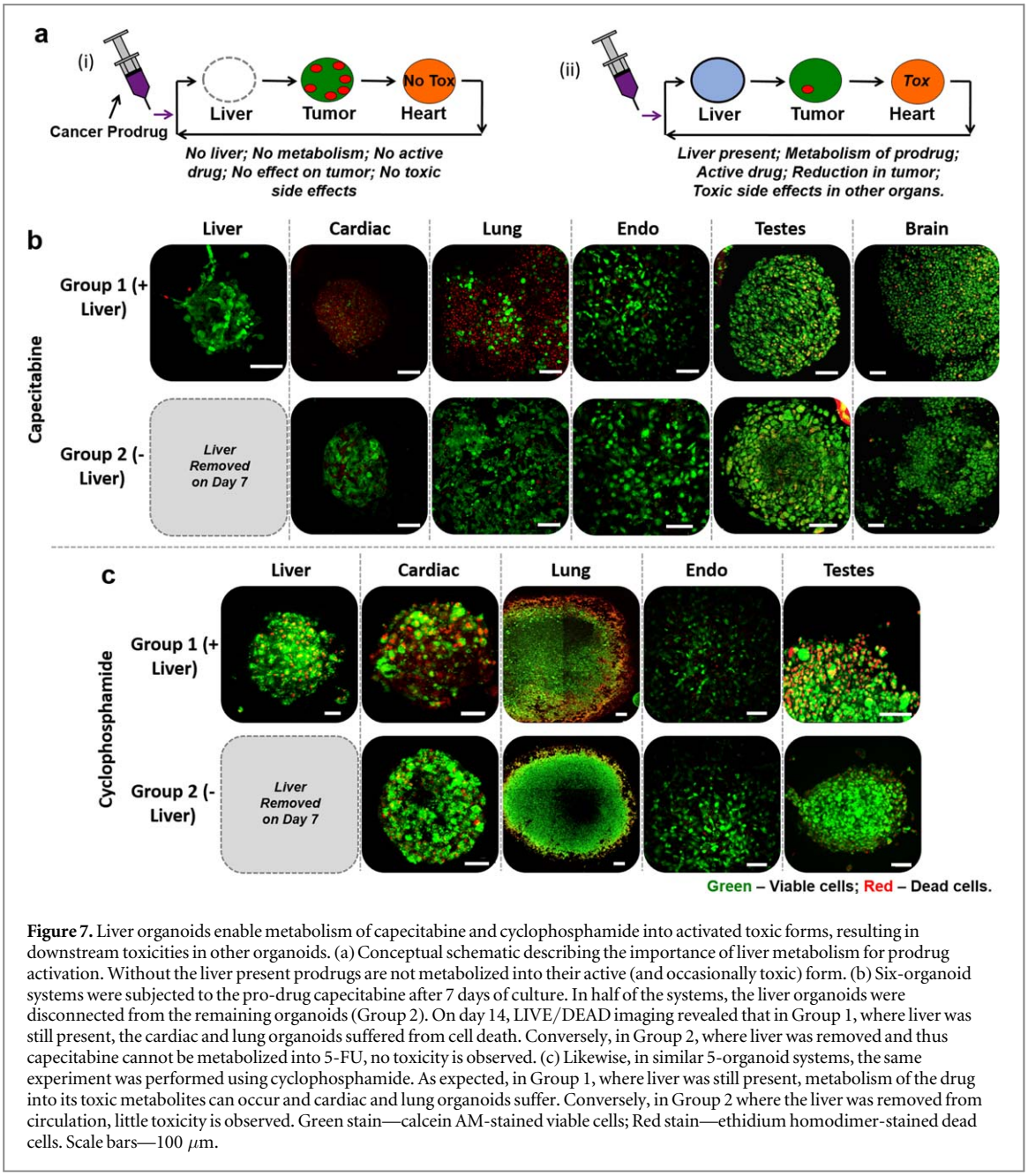

Figure 7. Liver organoids enable metabolism of capecitabine and cyclophosphamide into activated toxic forms, resulting in downstream toxicities in other organoids. (a) Conceptual schematic describing the importance of liver metabolism for prodrug activation. Without the liver present prodrugs are not metabolized into their active (and occasionally toxic) form. (b) Six-organoid systems were subjected to the pro-drug capecitabine after 7 days of culture. In half of the systems, the liver organoids were disconnected from the remaining organoids (Group 2). On day 14, LIVE/DEAD imaging revealed that in Group 1, where liver was still present, the cardiac and lung organoids suffered from cell death. Conversely, in Group 2, where liver was removed and thus capecitabine cannot be metabolized into 5-FU, no toxicity is observed. (c) Likewise, in similar 5-organoid systems, the same experiment was performed using cyclophosphamide. As expected, in Group 1, where liver was still present, metabolism of the drug into its toxic metabolites can occur and cardiac and lung organoids suffer. Conversely, in Group 2 where the liver was removed from circulation, little toxicity is observed. Green stain—calcein AM-stained viable cells; Red stain—ethidium homodimer-stained dead cells. Scale bars—100 μm.

developed as a non-sedative anti-histamine that was later recalled for causing arrhythmias [67]. Cisapride was developed as a gastroprokinetic agent for the treatment of gastroesophageal reflux disease and was later recalled for causing prolonged QT syndrome, leading to arrhythmia [68]. Mibefradil was developed as a calcium channel blocker to treat hypertension and was recalled for causing adverse interactions when combined with other medications [69, 70]. Pergolide was developed as a dopamine agonist for the treatment of Parkinson's disease and was recalled due to causing an increased risk of valvular heart disease [37]. Rofecoxib was developed as a NSAID COX-2 selective inhibitor for the treatment of pain caused by arthritis and acute pain and was recalled after causing tens of thousands of heart attacks [71]. Terodiline was developed as a drug to relax the bladder smooth muscle tissue for the treatment of incontinence and was later recalled for blocking IKr channels and therefore causing an increased risk for torsades de pointes [39]. Valdecoxib was developed as a NSAID COX-2 selective inhibitor for the treatment of arthritis and menstruation pain and was later recalled for causing an increase of heart attack, stroke and skin reactions [72]. Notably, organoid responses were compared among 3D tissue organoids, 2D analogs comprised of the same cells, 2D and 3D cell line-based analogs. Safe over the counter medications were also tested, showing no toxicity.

Second, we demonstrate the development of a platform that supports up to six distinct bioengineered organoid types—liver, cardiac, vascular, lung, testis, and colon or brain—within a single recirculating perfusion system under a common media (figures 5 and 6). We demonstrate the long-term maintenance of

viability in these systems, and show the utility of such integrated multi-tissue platforms by demonstrating different toxicity outcomes in response to capecitabine and cyclophosphamide depending whether or not liver organoids are present (figure 7).

The major driving force behind the development of *in vitro* organoid models is the need for advanced drug screening platforms that may more accurately predict drug efficacy and safety in humans [73, 74]. Importantly, these systems have the potential to identify toxic effects of drug candidates in development before they advance to clinical trials and are administered to patients. Unfortunately, a number of drugs pass clinical trials, reach the market, and are used by patients before it is recognized that they have detrimental side effects, and have to be recalled. If technologies such as body-on-a-chip platforms were well validated and utilized, these toxicities may have been identified earlier in development, In this context, we chose to demonstrate our platform utility by screening a panel of FDA-recalled drugs for toxic effects (figures 1–3). We successfully modeled liver toxicity from troglitazone and mibefradil and cardiac toxicity and beating rate decreases from astemizole, pergogide, and terodiline. Complications with the liver and heart account for approximately 90% of all drug failures and recalls, and as such, being able to demonstrate the ability to capture these outcomes is important. Our parallel studies using 2D control cultures and cell line studies further demonstrate the potential value of our platform. For example, in the case of liver, 2D cultures of primary hepatocytes and the commonly used HepG2 hepatoma cell line resulted in highly variable data, as compared to 3D tissue organoids. In some cases, the organoids were more sensitive and in some cases the organoids were more resistant to the drugs. These contrasting results—increased sensitivity to some drugs and increased resistance to others—indicate that the relationships between drug toxicity in the body versus 3D organoids versus 2D cultures are complex. The specific level of sensitivity for a given drug in 2D versus 3D likely depends on the mechanism of toxicity. We believe that this is due to several factors, such as the substantial surface area to volume ratio differences between 3D and 2D cultures. The buffering capacity to recover from small perturbances is also very different among 2D planar cultures, 250 μm spheres and clinical scale human organs. The effects of each of these differences would manifest differently based on the mechanism of toxicity for each drug tested. As such, we are currently investigating these factors and the specific mechanisms involved. These findings underscore not only the importance of using 3D cell systems for drug screening, but also the impact of preserving currently used 2D cell systems in order to have a more complete profile of potential adverse reactions. Additionally, we demonstrated that compounds typically considered non-toxic and available over the counter (aspirin, ibuprofen, ascorbic acid, loratadine, and quercetin) do not elicit toxic responses in these organoids, even at concentrations well above plasma levels documented in humans taking these compounds (figure 4).

Perhaps more relevant than individual organoid responses to drugs is a multi-organoid system response, in which the responses of one organoid may impact the responses in downstream organoids. Such integration moves the system closer to actual human physiology. When 6 tissue construct types were integrated within a single perfusion platform, relatively high viability in all 6 tissues types was maintained for 4 weeks. While other groups have demonstrated the capability to maintain multi-tissue model system viability for up to 4 weeks, these examples have been largely limited to 2D cultures or 3D cell lines [24, 60]. We had originally hypothesized that as each additional tissue type was added to the body-on-a-chip platform, a more complex media would be required to maintain cell viability and function. Surprisingly, this was found to not be the case. In 6-tissue platforms, the common media was biased towards what might be considered the more sensitive cells populations; specifically, the endothelial cells which were in a planar organization, and the testis organoids which requires specific and uncommon factors. Remarkably, we observed that the other 4 tissue types in the system performed well. Viability assays showed a very low rate of cell death. Soluble biomarker analysis revealed an initial spike in IL-8, prostacyclin, and in some systems CK, representing stress experienced by the lung, vascular, and cardiac constructs, respectively. However, over time, these biomarkers returned to levels present in media-only controls. This interesting result suggests that perhaps the presence of higher numbers of tissue types results in conditioning of the media towards a natural, supportive universal media; much like human serum. Additionally, once cells are placed in physiologically relevant 3D architectures, they may become internally supported through robust autocrine and paracrine signaling, and therefore less influenced by factors within the system medium. These theories are notable, because they suggest that multi-organoid platforms comprised of 3D tissue models may be able to move away from expensive tissue-specific media formulations currently on the market, and towards more inexpensive and simple common media. This finding in itself may be significant, but requires further assessment and testing.

One area of organoid study that is ripe for further development is quantitative pharmacokinetic and pharmacodynamic (PKPD) modeling. Despite the significant acceleration in development and application of *in vitro* 3D models for drug development, disease modeling, and personalized medicine, how one relates data from organoids and other bioengineered systems to the human population or individual human patient physiology remains an outstanding hurdle. The convergence of our 3D tissue construct platforms with such PKPD modeling in an area that our team is currently undertaking.

5. Conclusion

The work described herein demonstrates the creation of organoids and tissue constructs that show functionality similar to that derived of native human organs. The integration of six distinct bioengineered tissue models in single recirculating perfusion system, comprised of the liver, the heart, vasculature, lung, testis, and colon (or brain) is also demonstrated. Importantly, the individual components of the platform respond appropriately to a panel of drugs, including a variety of drugs that were removed from the market by the FDA due to toxicity in humans. Even more importantly, when combinations of organoids are combined into a single platform, more complex integrated responses can be observed, where the functionality of one organoid influenced the response of another organoid. This system, and others like it, based on 3D human-based tissue models with nuanced and complex response capabilities, has a great potential for influencing how *in vitro* drug and toxicology screening and disease modeling will be performed in the near future.

Acknowledgments

We thank Kalil Bitar (Wake Forest Institute for Regenerative Medicine) for providing rabbit colonic smooth muscle cells. The authors gratefully acknowledge funding by the Defense Threat Reduction Agency (DTRA) under Space and Naval Warfare Systems Center Pacific (SSC PACIFIC) Contract No. N6601-13-C-2027. The publication of this material does not constitute approval by the government of the findings or conclusions herein.

Competing interests

A S, T S, S S, S M, C B, and A A have filed patents pertaining to the results presented in the paper. The authors have no other competing interests to disclose.

ORCID iDs

Aleksander Skardal https://orcid.org/0000-0002-2138-2453
Julio Aleman https://orcid.org/0000-0001-7530-3303
Sean Murphy https://orcid.org/0000-0002-2820-2451

References

[1] Ciociola A A, Cohen L B and Kulkarni P 2014 How drugs are developed and approved by the FDA: current process and future directions *Am. J. Gastroenterol.* **109** 620–3
[2] Berenson A 2007 Merck Agrees to Settle Vioxx Suits for $4.85 Billion http://nytimes.com/2007/11/09/business/09merck.html
[3] Loftus P 2016 Merck to Pay $830 Million to Settle Vioxx Shareholder Suit https://wsj.com/articles/merck-to-pay-830-million-to-settle-vioxx-shareholder-suit-1452866882
[4] Tanne J H 2011 Merck pays $1bn penalty o promotion of rofecoxib *The BMJ* **343** d7702
[5] Whitstock M 2018 Manufacturing the truth: From designing clinical trials to publishing trial data *Indian J. Med. Ethics* **3** 152–3
[6] Kunz-Schughart L A, Freyer J P, Hofstaedter F and Ebner R 2004 The use of 3D cultures for high-throughput screening: the multicellular spheroid model *J. Biomol. Screen* **9** 273–85
[7] Ho W J *et al* 2010 Incorporation of multicellular spheroids into 3D polymeric scaffolds provides an improved tumor model for screening anticancer drugs *Cancer science* **101** 2637–43
[8] Drewitz M *et al* 2011 Towards automated production and drug sensitivity testing using scaffold-free spherical tumor microtissues *Biotechnol. J.* **6** 1488–96
[9] Skardal A *et al* 2017 Multi-tissue interactions in an integrated three-tissue organ-on-a-chip platform *Sci. Rep.* **7** 8837
[10] Skardal A *et al* 2012 Tissue specific synthetic ECM hydrogels for 3D *in vitro* maintenance of hepatocyte function *Biomaterials* **33** 4565–75
[11] Dobrolecki L E *et al* 2016 Patient-derived xenograft (PDX) models in basic and translational breast cancer research *Cancer Metastasis Rev.* **35** 547–73
[12] Wilke R A *et al* 2007 Identifying genetic risk factors for serious adverse drug reactions: current progress and challenges *Nat. Rev. Drug Discov.* **6** 904–16
[13] Okada J *et al* 2015 Screening system for drug-induced arrhythmogenic risk combining a patch clamp and heart simulator *Sci. Adv.* **1** e1400142
[14] Matsa E, Burridge P W and Wu J C 2014 Human stem cells for modeling heart disease and for drug discovery *Sci. Transl. Med.* **6** 239ps236
[15] Lai Y C, Chang W T, Lin K Y and Liau I 2014 Optical assessment of the cardiac rhythm of contracting cardiomyocytes *in vitro* and a pulsating heart *in vivo* for pharmacological screening *Biomed. Opt. Express* **5** 1616–25
[16] Meyer T, Leisgen C, Gonser B and Gunther E 2004 QT-screen: high-throughput cardiac safety pharmacology by extracellular electrophysiology on primary cardiac myocytes *Assay Drug Dev. Technol.* **2** 507–14
[17] Lynch T and Price A 2007 The effect of cytochrome P450 metabolism on drug response, interactions, and adverse effects *Am. Fam. Physician* **76** 391–6
[18] Zanger U M and Schwab M 2013 Cytochrome P450 enzymes in drug metabolism: regulation of gene expression, enzyme activities, and impact of genetic variation *Pharmacol. Ther.* **138** 103–41
[19] Smith M T 2003 Mechanisms of troglitazone hepatotoxicity *Chem. Res. Toxicol.* **16** 679–87
[20] Shen C, Meng Q and Zhang G 2012 Species-specific toxicity of troglitazone on rats and human by gel entrapped hepatocytes *Toxicol. Appl. Pharmacol.* **258** 19–25
[21] Marc Bedoucha E A and Boelsterli U A 2001 Diabetic KKAy mice exhibit increased hepatic PPARγ1 gene expression and develop hepatic steatosis upon chronic treatment with antidiabetic thiazolidinediones *J. Hepatology* **35** 6
[22] Skardal A, Devarasetty M, Forsythe S, Atala A and Soker S 2016 A reductionist metastasis-on-a-chip platform for *in vitro* tumor progression modeling and drug screening *Biotechnol. Bioeng.* **113** 2020–32
[23] Esch M B *et al* 2014 How multi-organ microdevices can help foster drug development *Adv. Drug Deliv. Rev.* **69-70** 158–69
[24] Oleaga C *et al* 2016 Multi-Organ toxicity demonstration in a functional human *in vitro* system composed of four organs *Sci. Rep.* **6** 20030
[25] Sung J H *et al* 2014 Using physiologically-based pharmacokinetic-guided 'body-on-a-chip' systems to predict mammalian response to drug and chemical exposure *Exp. Biol. Med.* **239** 1225–39
[26] Zhang Y S *et al* 2017 Multisensor-integrated organs-on-chips platform for automated and continual *in situ* monitoring of organoid behaviors *Proc. Natl Acad. Sci. USA* **114** E2293–302

[27] Edington C D *et al* 2018 Interconnected Microphysiological Systems for Quantitative Biology and Pharmacology Studies *Sci. Rep.* **8** 4530

[28] Aleman J and Skardal A 2018 A multi-site metastasis-on-a-chip microphysiological system for assessing metastatic preference of cancer cells *Biotechnol. Bioeng.* **116** 936–44

[29] Skardal A *et al* 2015 A hydrogel bioink toolkit for mimicking native tissue biochemical and mechanical properties in bioprinted tissue constructs *Acta Biomater.* **25** 24–34

[30] Pendergraft S S, Sadri-Ardekani H, Atala A and Bishop C E 2017 Three-dimensional testicular organoid: a novel tool for the study of human spermatogenesis and gonadotoxicity *in vitro Biol. Reprod.* **96** 720–32

[31] Nzou G *et al* 2018 Human cortex spheroid with a functional blood brain barrier for high-throughput neurotoxicity screening and disease modeling *Sci. Rep.* **8** 7413

[32] Hoppu K *et al* 1991 Accidental astemizole overdose in young children *Lancet* **338** 538–40

[33] Cools F *et al* 2003 A comparison of the pharmacokinetics of two dosing regimens of cisapride and their effects on corrected QT interval in premature infants *Eur. J. Clin. Pharmacol.* **59** 17–22

[34] Welker H A, Wiltshire H and Bullingham R 1998 Clinical pharmacokinetics of mibefradil *Clin. Pharmacokinet* **35** 405–23

[35] Mullins M E *et al* 1998 Life-threatening interaction of mibefradil and beta-blockers with dihydropyridine calcium channel blockers *JAMA* **280** 157–8

[36] Bowsher R R *et al* 1992 Sensitive, specific radioimmunoassay for quantifying pergolide in plasma *Clin. Chem.* **38** 1975–80

[37] Schade R, Andersohn F, Suissa S, Haverkamp W and Garbe E 2007 Dopamine agonists and the risk of cardiac-valve regurgitation *N. Engl. J. Med.* **356** 29–38

[38] Levesque L E, Brophy J M and Zhang B 2005 The risk for myocardial infarction with cyclooxygenase-2 inhibitors: a population study of elderly adults *Ann. Intern. Med.* **142** 481–9

[39] Thomas S H *et al* 1995 Concentration dependent cardiotoxicity of terodiline in patients treated for urinary incontinence *Br. Heart J.* **74** 53–6

[40] Skjodt N M and Davies N M 1999 Clinical pharmacokinetics and pharmacodynamics of bromfenac *Clin. Pharmacokinet* **36** 399–408

[41] Fontana R J *et al* 1999 Acute liver failure associated with prolonged use of bromfenac leading to liver transplantation. The acute liver failure study group *Liver Transpl. Surg.* **5** 480–4

[42] Neuberger J and Williams R 1989 Immune mechanisms in tienilic acid associated hepatotoxicity *Gut* **30** 515–9

[43] Yamazaki H *et al* 1999 Oxidation of troglitazone to a quinone-type metabolite catalyzed by cytochrome P-450 2C8 and P-450 3A4 in human liver microsomes *Drug Metab. Dispos.* **27** 1260–6

[44] Gitlin N, Julie N L, Spurr C L, Lim K N and Juarbe H M 1998 Two cases of severe clinical and histologic hepatotoxicity associated with troglitazone *Ann. Intern. Med.* **129** 36–8

[45] Skardal A, Devarasetty M, Rodman C, Atala A and Soker S 2015 Liver-tumor hybrid organoids for modeling tumor growth and drug response *in vitro Ann. Biomed. Eng.* **43** 2361–73

[46] Skardal A, Shupe T and Atala A 2016 Organoid-on-a-chip and body-on-a-chip systems for drug screening and disease modeling *Drug Discov. Today* **21** 1399–411

[47] Devarasetty M, Mazzocchi A R and Skardal A 2018 Applications of bioengineered 3D tissue and tumor organoids in drug development and precision medicine: current and future *BioDrugs* **32** 53–68

[48] Griffith L G and Swartz M A 2006 Capturing complex 3D tissue physiology *in vitro Nat. Rev. Mol. Cell Biol.* **7** 211–24

[49] Tibbitt M W and Anseth K S 2009 Hydrogels as extracellular matrix mimics for 3D cell culture *Biotechnol. Bioeng.* **103** 655–63

[50] Prestwich G D 2008 Evaluating drug efficacy and toxicology in three dimensions: using synthetic extracellular matrices in drug discovery *Acc. Chem. Res.* **41** 139–48

[51] Kosoglou T *et al* 2000 Evaluation of the pharmacokinetics and electrocardiographic pharmacodynamics of loratadine with concomitant administration of ketoconazole or cimetidine *Br. J. Clin. Pharmacol.* **50** 581–9

[52] Egert S *et al* 2008 Daily quercetin supplementation dose-dependently increases plasma quercetin concentrations in healthy humans *J. Nutr.* **138** 1615–21

[53] Ross-Lee L M *et al* 1982 Plasma levels of aspirin following effervescent and enteric coated tablets, and their effect on platelet function *Eur. J. Clin. Pharmacol.* **23** 545–51

[54] Xia Y and Whitesides G M 1998 Soft Lithography *Annu. Rev. Mater. Sci.* **28** 153–84

[55] Skardal A, Devarasetty M, Soker S and Hall A R 2015 *In situ* patterned micro 3D liver constructs for parallel toxicology testing in a fluidic device *Biofabrication* **7** 031001

[56] Gokaltun A, Yarmush M L, Asatekin A and Usta O B 2017 Recent advances in nonbiofouling PDMS surface modification strategies applicable to microfluidic technology *Technology (Singap World Sci)* **5** 1–12

[57] Devarasetty M, Skardal A, Cowdrick K, Marini F and Soker S 2017 Bioengineered Submucosal Organoids for *In Vitro* Modeling of Colorectal Cancer *Tissue Eng. Part A* **23** 1026–41

[58] Devarasetty M *et al* 2017 Optical tracking and digital quantification of beating behavior in bioengineered human cardiac organoids *Biosensors (Basel)* **7** 24

[59] Skardal A *et al* 2016 Bioprinting cellularized constructs using a tissue-specific hydrogel bioink *J. Vis. Exp.* **110** e53606

[60] Maschmeyer I *et al* 2015 A four-organ-chip for interconnected long-term co-culture of human intestine, liver, skin and kidney equivalents *Lab Chip* **15** 2688–99

[61] Hunter E B, Johnston P E, Tanner G, Pinson C W and Awad J A 1999 Bromfenac (Duract)-associated hepatic failure requiring liver transplantation *Am J Gastroenterol* **94** 2299–301

[62] Lopez-Garcia M P, Dansette P M and Mansuy D 1994 Thiophene derivatives as new mechanism-based inhibitors of cytochromes P-450: Inactivation of yeast-expressed human liver cytochrome P-450 2C9 by tienilic acid *Biochemistry* **33** 166–75

[63] Takagi S, Takayama S and Onodera T 1991 Hepatotoxicity of DR-3438, tienilic acid, indacrinone and furosemide studied *in vitro Toxicol. Lett.* **55** 287–93

[64] Manier J W C, William W L, Kirchner and John P 1982 Beltaos, efstathio. hepatotoxicity associated with ticrynafen–A uricosuric diuretic *Am. J. Gastroenterol.* **77**

[65] Aljada A *et al* 2001 Nuclear factor-kappaB suppressive and inhibitor-kappaB stimulatory effects of troglitazone in obese patients with type 2 diabetes: evidence of an antiinflammatory action? *J. Clin. Endocrinol. Metab.* **86** 3250–6

[66] Cohen J S 2006 Risks of troglitazone apparent before approval in USA *Diabetologia* **49** 1454–5

[67] Zhou Z, Vorperian V R, Gong Q, Zhang S and January C T 1999 Block of HERG potassium channels by the antihistamine astemizole and its metabolites desmethylastemizole and norastemizole *J. Cardiovasc. Electrophysiol.* **10** 836–43

[68] Gheuens J 2000 Propulsid (cisapride) *Safety Information* (New Jersey: Janssen Pharmaceuticals)

[69] Billups S J and Carter B L 1998 Mibefradil withdrawn from the market *Ann. Pharmacother.* **32** 841

[70] Po A L and Zhang W Y 1998 What lessons can be learnt from withdrawal of mibefradil from the market? *Lancet* **351** 2

[71] Fosslien E 2005 Cardiovascular complications of non-steroidal anti-inflammatory drugs *Ann. Clin. Lab. Sci.* **35** 347–85

[72] Zhang J, Ding E L and Song Y 2006 Adverse effects of cyclooxygenase 2 inhibitors on renal and arrhythmia events: meta-analysis of randomized trials *JAMA* **296** 1619–32

[73] Benam K H *et al* 2015 Engineered *in vitro* disease models *Ann. Rev. Pathol.* **10** 195–262

[74] Polini A *et al* 2014 Organs-on-a-chip: a new tool for drug discovery *Expert Opin. Drug Discovery* **9** 335–52

[75] DiMasi J A, Grabowski H G and Hansen R W 2016 Innovation in the pharmaceutical industry: new estimates of R&D costs *J. Health Econ.* **47** 20–33

[76] Regulatory Focus 2014 Number of Drug Recalls Surges at FDA, led by Mid-Level Concerns (http://raps.org/Regulatory-Focus/News/2014/08/11/20005/Number-of-Drug-Recalls-Surges-at-FDA-Led-by-Mid-Level-Concerns)